Applied Physics Letters ARTICLE scitation.org/journal/apl

Spin-orbit torque and Dzyaloshinskii–Moriya interaction in 4*d* metal Rh-based magnetic heterostructures

Cite as: Appl. Phys. Lett. **118**, 112402 (2021); doi: 10.1063/5.0034708
Submitted: 22 October 2020 · Accepted: 6 March 2021 ·
Published Online: 15 March 2021

View Online Export Citation CrossMark

Cuimei Cao,[1] Shiwei Chen,[2] Wenjie Song,[3] Xiaoyan Zhu,[1] Shuai Hu,[2] Xuepeng Qiu,[2] Guozhi Chai,[3] Lin Sun,[1] Wenjuan Cheng,[1] Dongmei Jiang,[1] and Qingfeng Zhan[1,a)]

AFFILIATIONS

[1]Key Laboratory of Polar Materials and Devices (MOE) and State Key Laboratory of Precision Spectroscopy, School of Physics and Electronic Science, East China Normal University, Shanghai 200241, People's Republic of China
[2]Shanghai Key Laboratory of Special Artificial Microstructure Materials, School of Physics Science and Engineering, Tongji University, Shanghai 200092, People's Republic of China
[3]Key Laboratory for Magnetism and Magnetic Materials (MOE), Lanzhou University, Lanzhou 730000, People's Republic of China

[a)]Author to whom correspondence should be addressed: qfzhan@phy.ecnu.edu.cn

ABSTRACT

The electrical switching of magnetization through spin–orbit torque (SOT) has potential applications for energy-efficient spintronic devices. Previous studies focused mostly on 5*d* heavy metals with strong spin–orbit coupling (SOC) to generate a spin current or a nonequilibrium spin accumulation and exert SOTs on the magnetization of a neighboring ferromagnetic layer. Recent theoretical and experimental studies indicated that 4*d* metals with weak SOC may also generate a sizable torque and realize the current-induced magnetization switching. In this work, we studied the current-induced SOTs in 4*d* metal Rh-based magnetic heterostructures with a perpendicular magnetic anisotropy. The damping-like SOT efficiency ξ_{DL} of $[Ni/Co]_3/Rh$ multilayers increases with the Rh thickness t_{Rh} and becomes saturated at $t_{Rh} = 5$ nm. Although the spin-Hall angle of Rh is rather small about 0.028 ± 0.005, a reversible current-induced SOT switching can still be achieved. In addition, the interfacial Dzyaloshinskii-Moriya interaction (iDMI) in Rh/Co heterostructures was quantitatively characterized by using Brillouin light scattering. The iDMI constant D increases with t_{Rh} and reaches 224 ± 39 $\mu J/m^2$ at $t_{Rh} = 5$ nm. Our results indicated that even for a weak SOC 4*d* metal Rh, it is still possible to obtain a current-induced magnetization switching and observe an obvious iDMI effect in the Rh-based magnetic heterostructures, which may broaden the scope of spintronic materials used for SOT devices.

Manipulation of the magnetization direction via the interaction between spins and charges is the core issue for spintronic devices. Recently, the controllable magnetization switching and domain-wall (DW) motion via the spin–orbit torques (SOTs) in nonmagnetic metal/ferromagnetic metal (NM/FM) heterostructures have attracted increasing interest for their potential applications in magnetic memory and logic devices.[1–6] The mechanism of SOTs in NM/FM heterostructures is that an injected charge current in the NM layer is converted into a spin current or a nonequilibrium spin accumulation due to the spin-Hall effect (SHE)[2,7] and/or the Rashba-Edelstein effect;[1,8] then, the spin angular momentum can be transferred from the spin current to the neighboring FM layer, exerting SOTs on the atomic spins. The conversion efficiency from a charge current j_c to a spin current j_s in NM layers is defined as the spin-Hall angle $\theta_{SH} = (2e/\hbar)j_s/j_c$, where e and $\hbar$ are the elementary charge and the Planck constant, respectively.[9] Therefore, the studies about the θ_{SH} value of NM layers are essential for the low power operation of spintronic memory and logic devices based on the SOTs.

The interfacial Dzyaloshinskii–Moriya interaction (iDMI) refers to a short-range antisymmetric exchange interaction, which results from the spin–orbit coupling (SOC) in NM/FM heterostructures with broken inversion symmetry and favors a non-collinear alignment of neighboring spins.[10–13] The conventional picture of the iDMI in NM/FM heterostructures is due to a 3-site indirect exchange coupling between two atomic spins $\boldsymbol{S}_1$ and $\boldsymbol{S}_2$ via a neighboring atom having a SOC.[12–14] $\boldsymbol{S}_1$ and $\boldsymbol{S}_2$ in the FM layer couple to each other through the overlap of their wave functions with an atom with SOC in the NM layer. This overlap gives rise to a contribution to the DMI energy in

the form $\boldsymbol{D}_{12}\cdot(\boldsymbol{S}_1 \times \boldsymbol{S}_2)$, where the iDMI vector $\boldsymbol{D}_{12}$ lies in the interface plane with the direction normal to the plane defined by the three atoms. The existence of such an interfacial DMI has also been derived from *ab initio* calculations for the Ir(111)/Fe and Rh/Co/Pt heterojunction.[15–17] The iDMI can stabilize chiral spin structures such as Néel-type DWs whose spin texture enables an extremely efficient SOT-driven DW motion and can play an important role in the SOT-induced magnetization switching.[4,18–20] Thus, it is another important factor for designing SOT spintronics devices.

So far, most relevant studies of SOTs[2,3,21–24] and iDMI[24–27] focused mostly on 5*d* heavy metals with a strong SOC, a high charge-to-spin conversion efficiency, and a large iDMI constant. However, less attention was paid to study relatively light elements due to the expected weak SOC. Previous theories have predicted that the orbital Hall effect (OHE), which is the transverse flow of orbital angular momentum caused by an applied electric field, can occur in 3*d* and 4*d* metals despite the weak SOC and generate an extra torque to assist the current-induced magnetization switching.[28–31] More recently, the SOT-induced magnetization switching has been achieved in 3*d* and 4*d* metals, such as Mo-,[32] Cr-,[33] Zr-,[34] Ru-,[35] and CoFeB-based[36] multilayers with a perpendicular magnetic anisotropy (PMA). Theoretical calculations indicated that the 4*d* metal Rh possesses a considerable SOC strength and a large spin-Hall conductivity.[30] As a result, a significant spin-Hall magnetoresistance (SMR) of 7×10^{-5} has been observed in the Rh/$Y_3Fe_5O_{12}$ heterojunctions with a negligible magnetic proximity effect at 300 K.[37] Additionally, the theoretical calculation has predicted that the orbital Hall conductivity of Rh is approximately $\sim 3 \times 10^3\ \Omega^{-1}\,\mathrm{cm}^{-1}$, which is larger than the values of most of the 5*d* metals.[28,29] However, systematic works on the SOTs and iDMI of 4*d* metal Rh-based heterostructures are still lacking. In the present work, we quantitatively studied the SOT efficiency and iDMI constant in Rh/FM heterostructures with varying the Rh thickness t_{Rh}. We obtained a PMA and realized the current-induced magnetization switching in Ta/Cu/$[Ni/Co]_3$/Rh/SiO_2 multilayers with different t_{Rh}. The damping-like SOT efficiency ξ_{DL} increases with t_{Rh} and becomes saturated at $t_{Rh} = 5$ nm. The spin-Hall angle of Rh is obtained as $\theta_{SH} = 0.028 \pm 0.005$. In addition, Rh/Co/MgO/TaO_x multilayers with an in-plane magnetic anisotropy were fabricated to investigate the iDMI. The iDMI constant D of the Rh/Co interface increases with t_{Rh} and reaches 224 ± 39 μJ/m^2 at $t_{Rh} = 5$ nm. Both the damping-like SOT efficiency and the iDMI constant display a similar dependence on t_{Rh}, which indicates that both effects originate from the indirect interaction between the NM and FM atoms mediated by the itinerant electron spins.

Multilayer structures of Ta(2)/Cu(3)/$[Ni(0.3)/Co(0.15)]_3$/Rh(*t*)/SiO_2(2) and Rh(*t*)/Co(2)/MgO(2)/TaO_x(2), where the numbers in parentheses represent the nominal thicknesses in nanometers, were fabricated on thermally oxidized Si substrates at room temperature by using an ultrahigh-vacuum magnetron sputtering system with a base pressure better than 1.0×10^{-5} Pa. The capping layers of SiO_2 and TaO_x were used to protect the samples from oxidation. The buffer layers of Ta/Cu are the seed layer to promote the (111) texture and induce a PMA in $[Ni/Co]_3$ multilayers. The 3 nm Cu layer is thick enough to cut off the spin current flowing from the bottom Ta layer. Subsequently, the Ta(2)/Cu(3)/$[Ni(0.3)/Co(0.15)]_3$/Rh(*t*)/SiO_2(2) films were patterned into a Hall-bar geometry with an 8 μm width and a 50 μm length by conventional photolithography and Ar-ion-beam etching, as shown in Fig. 1(a). The film thicknesses were controlled by the deposition time, which have been calibrated by x-ray reflectivity (XRR). The typical error on thicknesses is less than 4%.

The anomalous Hall effect (AHE) and the harmonic Hall voltages were measured using a combination of a Keithley 6221 current source, a Keithley 2182 nanovoltmeter, and two Stanford S830 lock-in amplifiers, where a pulse current was applied along the *x* axis of the Hall bar and the voltage was obtained along the *y* axis. The magnetic hysteresis loops (*M*-*H*) were measured by a magnetic property measurement system (MPMS, Quantum Design). The iDMI constants in the Rh(*t*)/Co/MgO/TaO_x multilayers were determined through the measurement of the asymmetric spin wave by using the Brillouin light scattering (BLS) technique. All measurements were conducted at room temperature.

Figure 1(b) shows the static magnetic characteristics for the typical $[Ni/Co]_3$/Rh(4.5 nm) heterostructure with the magnetic field applied perpendicular and parallel to the film plane. The out-of-plane magnetic hysteresis loop is relatively square with a coercive field of 18.0 ± 0.1 mT and a saturation magnetization of $(9.56 \pm 0.05) \times 10^5$ A/m, indicating a remarkable PMA. The slanted in-plane magnetic hysteresis loop indicates the PMA anisotropy field $\mu_0 H_k = 0.75 \pm 0.07$ T. The anomalous Hall resistance R_{AHE} by subtracting the offset as a function of the out-of-plane magnetic field H_z for the $[Ni/Co]_3$/Rh(4.5 nm) sample follows a square loop with the saturation $R_{AHE} = 30.0 \pm 0.2$ mΩ, as shown in the inset of Fig. 1(b). An exemplary current-induced magnetization switching is measured with a 100 μs pulse current applied along the *x* direction. The pulse current is used to reduce the Joule heating effect. A bias magnetic field H_x of 40 mT is applied along the current direction to break the symmetry of magnetization switching, thereby setting the deterministic switching polarities. The current density j_{Rh} in the Rh layer is evaluated by considering the shunting effect of metallic layers with a relation $j_{Rh} = I[\rho_{Ta/Cu/[Ni/Co]_3} t_{Rh}/(\rho_{Ta/Cu/[Ni/Co]_3} t_{Rh} + \rho_{Rh} t_{Ta/Cu/[Ni/Co]_3})]/w t_{Rh}$,[32] where I is the current applied to the multilayered devices, w is the width of the Hall bar channel, and t_{Rh} and $t_{Ta/Cu/[Ni/Co]_3}$ are the thicknesses of the Rh and Ta/Cu/$[Ni/Co]_3$ layers, respectively. The resistivities ρ of Rh(4.5) and Ta(2)/Cu(3)/$[Ni(0.3)/Co(0.15)]_3$ are obtained by measuring the Rh(4.5)/SiO_2(2) and Ta(2)/Cu(3)/$[Ni(0.3)/Co(0.15)]_3$/SiO_2(2) samples with the four-probe method, which gives $\rho_{Rh} = 56.6 \pm 2.9$ $\mu\Omega$ cm and $\rho_{Ta/Cu/[Ni/Co]_3} = 93.4 \pm 3.2$ $\mu\Omega$ cm. Figure 1(c) representatively shows the current-induced magnetization switching along the *z* axis for the $[Ni/Co]_3$/Rh(4.5 nm) multilayer. When the current density j_{Rh} is swept from $(9.3 \pm 0.3) \times 10^7$ to $(-9.3 \pm 0.3) \times 10^7$ A/cm^2, R_{AHE} can be switched from 22.1 ± 0.2 to -22.1 ± 0.2 mΩ, indicating the orientation of magnetization is changed from up to down. In comparison with the saturation R_{AHE}, the pulse current approximately induces a switching of 74% magnetization, which is probably because the reduced current density at the edge of Hall cross falls below the threshold.[38] The critical current density in the Rh layer induces a magnetization switching of $(6.8 \pm 0.2) \times 10^7$ A/cm^2, which is close to the value obtained in the 4*d* metal Mo-based magnetic heterostructures.[30] The magnetization switching curve changes its switching polarity when the direction of the bias field is reversed, displaying a typical characteristic of the SOT switching of PMA films.[3]

For the current-induced magnetization switching in FM/NM heterostructures, the SOT-induced effective field exerted on the magnetic moments can be decomposed into two components, namely, the damping-like effective field H_{DL} ($\boldsymbol{\sigma} \times \boldsymbol{m}$) and the field-like effective

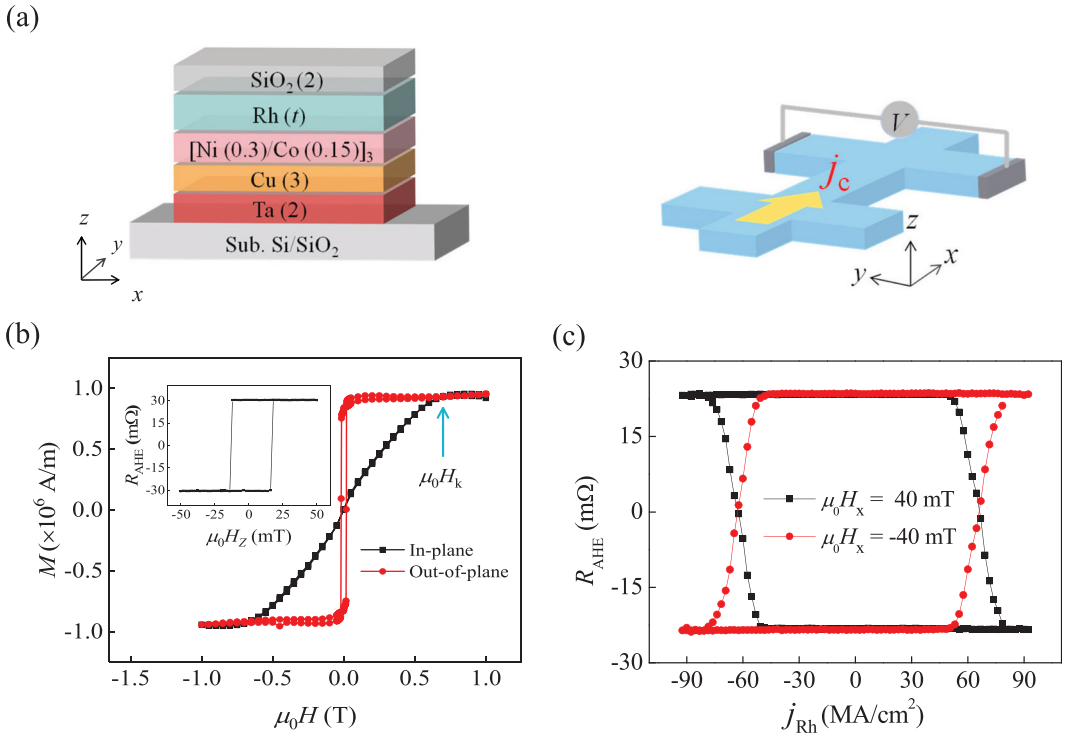

FIG. 1. (a) Schematics of the layer structure of Ta(2)/Cu(3)/[Ni(0.3)/Co(0.15)]$_3$/Rh(t)/SiO$_2$(2) multilayers and the measurement configurations for the anomalous Hall resistances and the harmonic Hall voltages. (b) Magnetic hysteresis curves for the typical [Ni/Co]$_3$/Rh(4.5 nm) heterostructure measured with an in-plane or out-of-plane magnetic field. The inset shows the corresponding anomalous Hall resistance as a function of the out-of-plane magnetic field. (c) The representative current-induced magnetization switching along the z axis for the [Ni/Co]$_3$/Rh(4.5 nm) multilayer with applying an in-plane magnetic field of 40 mT along the x and -x axes.

field H_{FL} ($\boldsymbol{\sigma}$), where $\boldsymbol{\sigma}$ and $\boldsymbol{m}$ are the unit vectors of the spin polarization direction in the NM layer and magnetization in the FM layer, respectively. In order to quantitatively evaluate the current-induced effective fields, harmonic Hall voltage measurements are performed in two configurations. An ac current with a low frequency of 13.7 Hz is passed into the patterned Hall bars along the x direction, while an in-plane magnetic field is swept along either the longitudinal (H_x) or transverse (H_y) direction; then, the first ($V_{1\omega}$) and second ($V_{2\omega}$) harmonic Hall voltages are recorded by two lock-in amplifiers. Figure 2 shows the representative in-plane magnetic field dependencies of the harmonic Hall voltages of $V_{1\omega}$ and $V_{2\omega}$ for the [Ni/Co]$_3$/Rh(4.5 nm) sample when an ac current of $j_{Rh} = (9.2 \pm 0.3) \times 10^6$ A/cm^2 is applied along the x direction. $V_{1\omega}$ displays a parabola dependence on H_x and H_y for the magnetization along the $+z$ and $-z$ directions after subtracting the offset, as shown in Figs. 2(a) and 2(c), respectively. $V_{2\omega}$ reveals a linear dependence on H_x and H_y. The slopes of $V_{2\omega}$ vs H_x are identical for the magnetization along the $+z$ and $-z$ directions, as shown in Fig. 2(b). In contrast, the absolute values of the slopes of $V_{2\omega}$ vs H_y are the same for the magnetization along the $+z$ and $-z$ directions, but their signs are opposite, as shown in Fig. 2(d). The damping-like effective field H_{DL} and the field-like effective field H_{FL} can be quantitatively obtained according to the measurement of harmonic Hall voltages,[39,40]

$$\mu_0 H_{DL(FL)} = -2\frac{(B_{x(y)} \pm 2\xi B_{y(x)})}{1 - 4\xi^2}, \tag{1}$$

where $B_x \equiv -2\frac{\partial V_{2\omega}}{\partial H_x} / \frac{\partial^2 V_{1\omega}}{\partial H_x^2}$, $B_y \equiv -2\frac{\partial V_{2\omega}}{\partial H_y} / \frac{\partial^2 V_{1\omega}}{\partial H_y^2}$, the $\pm$ sign of $B_{y(x)}$ corresponds to the magnetization along the $+z$ and $-z$ directions, and ξ is the ratio of the planar Hall resistance R_{PHE} to the anomalous Hall resistance R_{AHE}. Figure 3(a) shows the azimuthal angle φ dependence of Hall resistance R_H for the [Ni/Co]$_3$/Rh(4.5 nm) sample with an in-plane magnetic field of 1.5 T applied to saturate the magnetization in the film plane. Consequently, $R_{PHE} = 6.05 \pm 0.02$ mΩ can be obtained by fitting to the equation of $R_H = \frac{1}{2} R_{PHE} \sin 2\varphi$ and the ξ is approximately 20%. According to the fitting to Eq. (1), both H_{DL} and H_{FL} as a function of j_{Rh} for the [Ni/Co]$_3$/Rh(4.5 nm) sample can be obtained, as shown in Figs. 3(b) and 3(c), respectively. The linear dependence of the effective fields on j_{Rh} indicates that the effect of Joule heating is negligible within the range of applied j_{Rh}. The damping-like SOT efficiency ξ_{DL}, which describes the magnitude of damping-like effective field exerted on the FM moments under a unit current density in the NM layer, can be estimated by using the expression:[41]

$$\xi_{DL} = 2eM_s t_{FM} H_{DL} / \hbar j_{Rh}, \tag{2}$$

where t_{FM} represents the total thickness of the [Co/Ni]$_3$ layer. The Rh layer resistivities ρ_{Rh} as a function of t_{Rh} are shown in the inset of Fig. 3(d) to determine j_{Rh} in Ta(2)/Cu(3)/[Ni(0.3)/Co(0.15)]$_3$/Rh(t)/SiO$_2$(2) samples. The phenomenon that ρ_{Rh} increases with decreasing t_{Rh} can be explained by the strong diffusive scattering at a Rh surface.[42,43] The obtained value of ξ_{DL} increases with t_{Rh} and becomes saturated at $t_{Rh} = 5$ nm, as shown in Fig. 3(d). The t_{Rh} dependence of

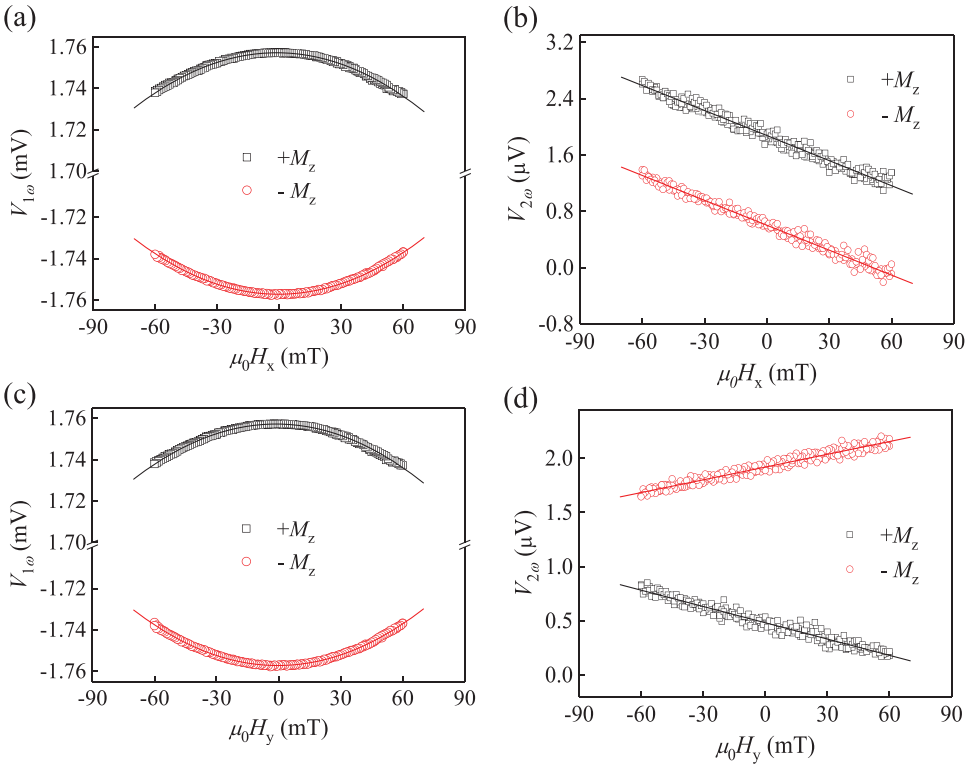

FIG. 2. The first harmonic Hall voltages $V_{1\omega}$ as a function of (a) the longitudinal magnetic field $\mu_0 H_x$ and (c) the transverse magnetic field $\mu_0 H_y$ for the $[Ni/Co]_3$/Rh(4.5 nm) heterostructure magnetized along the $+z$ and $-z$ directions. The second harmonic voltages $V_{2\omega}$ vs (b) $\mu_0 H_x$ and (d) $\mu_0 H_y$ for the sample magnetized along the $+z$ and $-z$ directions. The hollow symbols and the solid lines represent the experimental data and the fitting results, respectively.

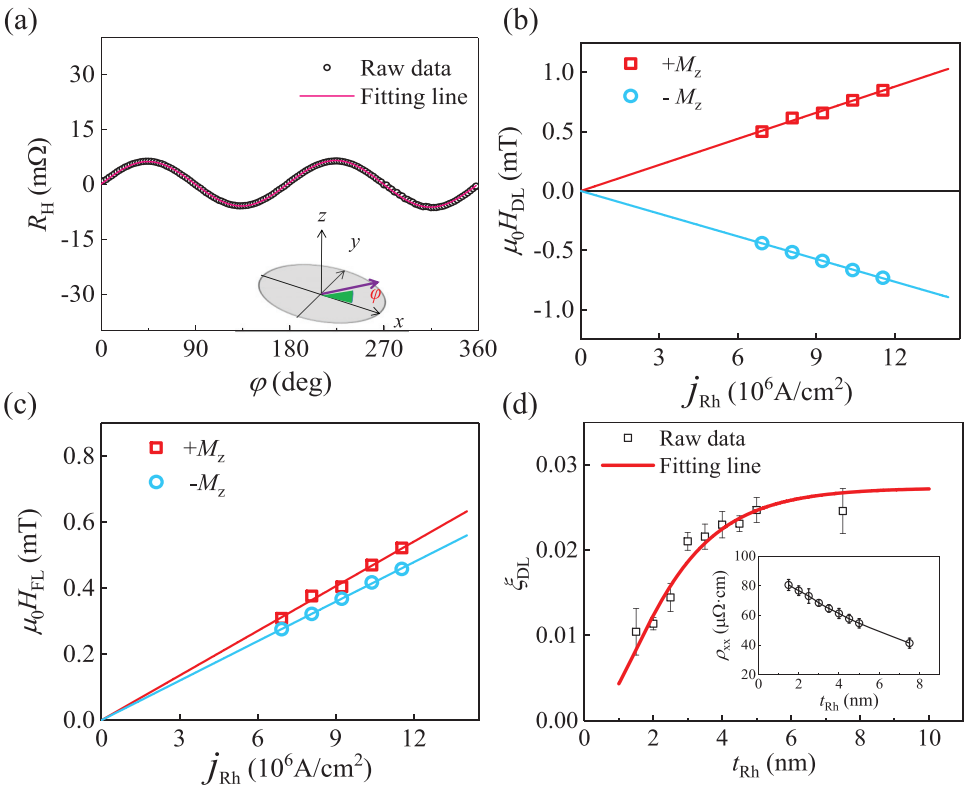

FIG. 3. (a) The azimuthal angle φ dependence of Hall resistance R_H for the $[Ni/Co]_3$/Rh(4.5 nm) sample with a magnetic field of 1.5 T applied to saturate the magnetization in the film plane. The solid line is the theoretical fitting curve. (b) The damping-like effective field $\mu_0 H_{DL}$ and (c) the field-like effective field $\mu_0 H_{FL}$ as a function of the current density in the Rh layer for the $[Ni/Co]_3$/Rh(4.5 nm) sample magnetized along the $+z$ and $-z$ directions. The solid lines are the linear fitting of the data. (d) The Rh thickness dependence of the damping-like SOT efficiency ξ_{DL} for the $[Ni/Co]_3$/Rh multilayers with different t_{Rh} and the inset shows the Rh layer resistivities ρ_{Rh} as a function of t_{Rh}. The solid line is the fitting result using the simplest drift diffusion model.

ξ_{DL} can be interpreted by the bulk contribution of the SHE. For a NM/FM heterostructure, the spin current is generated by the bulk SHE in the NM layer and is entirely absorbed at the NM/FM interface; the simplest drift diffusion model gives the t_{Rh} dependence of ξ_{DL} as[42]

$$\xi_{DL} = \theta_{SH}[1 - \mathrm{sech}(t_{Rh}/\lambda_s)], \quad (3)$$

where λ_s is the spin diffusion length. The fitting to the drift diffusion model shows good agreement with the experimental results, which yields $\theta_{SH} = 0.028 \pm 0.005$ and $\lambda_s = 1.7 \pm 0.3$ nm. The spin-Hall angle of Rh is obviously smaller than that of the well-studied metals Pt,[44] Ta,[2] and W[9] due to the rather weak SOC.

Previously, Di *et al.* observed a frequency shift in the BLS measurement for MgO/Co/Ni/MgO/SiO_2 samples, which is attributed to the existence of asymmetric surface anisotropy and/or an iDMI at the Co/Ni interface.[45] In order to demonstrate the iDMI of the Rh/Co interface and avoid the possible iDMI induced by the Cu/Co and Co/Ni interfaces,[45,46] we, therefore, fabricated the heterostructures of Rh/Co/MgO/TaO_x with different Rh thicknesses for the BLS measurements. Figure 4(a) depicts the schematic of the BLS measurement for the iDMI constant D with an external bias magnetic field applied along the y direction. An s-polarized monochromatic laser beam with a wavelength $\lambda = 532$ nm is focused on the Rh/Co/MgO/TaO_x sample surface with an incident angle θ. The p-polarized backscattered light is collected and sent to a Sandercock-type $(3+3)$-pass tandem Fabry–Pérot interferometer. The Stokes and anti-Stokes peaks in BLS spectra correspond to the creation and annihilation of magnons with in-plane wave vector $k_x = \frac{4\pi}{\lambda}\sin\theta$, denoting the projection of the magnon wave vector in the x direction. Figure 4(b) shows the typical BLS spectra of Rh(4.5 nm)/Co/MgO/TaO_x. Owing to the presence of iDMI in the sample, the difference in frequency between the Stokes and anti-Stokes peaks can be observed, which relates to the reversal of the spatial chirality of spin wave in k_x space. In order to quantify the iDMI constant D, BLS measurements are performed through varying the incident angle to change the wave vector k_x. Figure 4(c) plots the iDMI-induced frequency shift f_{dm} as a function of k_x for the Rh/Co/MgO/TaO_x multilayers with different t_{Rh}. The iDMI constant D for the Rh/Co/MgO/TaO_x samples can be obtained, as described in Fig. 4(d), by the linear fitting to the relation $f_{dm} = \frac{2\gamma}{\pi M_s} D k_x$,[47] where the gyromagnetic ratio $\gamma = 176 \pm 2$ GHz/T and the saturation magnetization of Co $M_s = (1.20 \pm 0.06) \times 10^6$ A/m obtained by the MPMS measurement. As shown in Fig. 4(d), more and more Rh atoms provide SOC interaction with increasing the thickness of HM layer Rh, and iDMI constant D continues to increase and finally tends to saturation, which is 224 ± 39 μJ/m^2 when $t_{Rh} = 5$ nm. The iDMI constant of Rh/Co is one order of magnitude less than that of the Pt/Co interface (1586 μJ/m^2),[45] but it is comparable with that in the other bilayers of Ta/Co (81 μJ/m^2), W/Co (111 μJ/m^2), Ir/Co (335 μJ/m^2), Cr/CoFeB (250 μJ/m^2), and Mo/CoFeB (350 μJ/m^2).[30,31,48] This result may give the evidence that iDMI originates from the indirect interaction between HM atoms with large SOC and the FM spin mediated by the itinerant electron spin.

In summary, we investigated the SOT and iDMI effects in the 4d metal Rh-based magnetic heterostructures. The SOT-induced magnetization switching was demonstrated in the $[Ni/Co]_3$/Rh multilayers

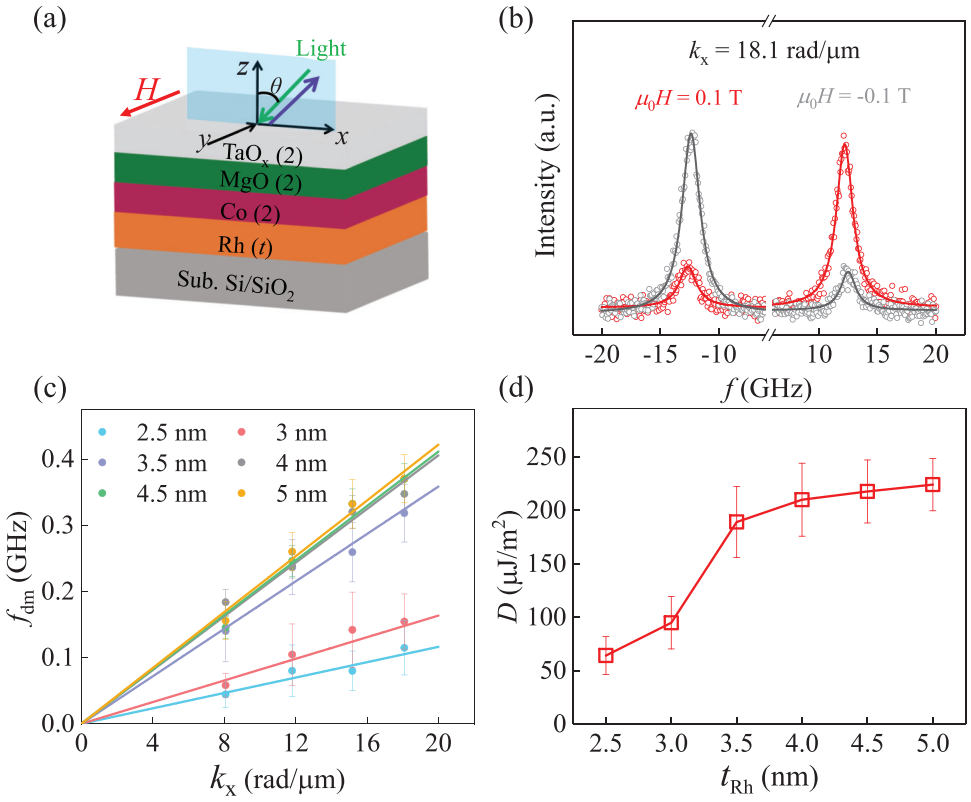

FIG. 4. (a) Schematics of the BLS measurement for the iDMI constant of Rh/Co/MgO/TaO_x multilayers with an external bias magnetic field applied along the y direction. (b) The typical BLS spectra of Rh(4.5 nm)/Co/MgO/TaO_x measured with in-plane wave vector $k_x = 18.1$ rad/μm under oppositely oriented external magnetic fields. (c) The iDMI-induced frequency shift f_{dm} as a function of k_x for the Rh/Co/MgO/TaO_x multilayers with different t_{Rh}. The solid lines are the linear fitting of the data. (d) The obtained iDMI constant D for the Rh/Co/MgO/TaO_x samples with different t_{Rh}.

with a PMA. The damping-like SOT efficiency ξ_{DL} increases with t_{Rh} and becomes saturated at $t_{Rh} = 5$ nm. The spin-Hall angle θ_{SH} of Rh is obtained approximately 0.028 ± 0.005, which is obviously smaller than that of the well-studied 5*d* metals due to the rather weak SOC. The iDMI effect of the Rh/Co interfaces was quantitatively studied by BLS. The iDMI constant D increases with t_{Rh} and reaches 224 ± 39 $\mu J/m^2$ at $t_{Rh} = 5$ nm. Both ξ_{DL} and D display a similar dependence on t_{Rh}, which indicates that both current-induced SOTs and iDMI originate from a similar indirect interaction between the NM and FM atoms mediated by the itinerant electron spins.

AUTHORS' CONTRIBUTIONS

C.C. and S.C. contributed equally to this work.

This work was financially supported by the National Natural Science foundation of China (Nos. 11674336 and 11874150). ECNU Public Platform for Innovation provides MPMS for the measurement of magnetic properties.

DATA AVAILABILITY

The data used to support the findings of this study are available from the corresponding author upon request.

REFERENCES

[1]I. M. Miron, K. Garello, G. Gaudin, P. J. Zermatten, M. V. Costache, S. Auffret, S. Bandiera, B. Rodmacq, A. Schuhl, and P. Gambardella, Nature **476**, 189 (2011).
[2]L. Liu, C. F. Pai, Y. Li, H. W. Tseng, D. C. Ralph, and R. A. Buhrman, Science **336**, 555 (2012).
[3]L. Liu, O. J. Lee, T. J. Gudmundsen, D. C. Ralph, and R. A. Buhrman, Phys. Rev. Lett. **109**, 096602 (2012).
[4]S. Emori, U. Bauer, S. M. Ahn, E. Martinez, and G. S. Beach, Nat. Mater. **12**, 611 (2013).
[5]P. P. J. Haazen, E. Mure, J. H. Franken, R. Lavrijsen, H. J. Swagten, and B. Koopmans, Nat. Mater. **12**, 299 (2013).
[6]K. S. Ryu, L. Thomas, S. H. Yang, and S. Parkin, Nat. Nanotechnol. **8**, 527 (2013).
[7]J. E. Hirsch, Phys. Rev. Lett. **83**, 1834 (1999).
[8]D. A. Pesin and A. H. MacDonald, Phys. Rev. B **86**, 014416 (2012).
[9]C. F. Pai, L. Liu, Y. Li, H. W. Tseng, D. C. Ralph, and R. A. Buhrman, Appl. Phys. Lett. **101**, 122404 (2012).
[10]I. Dzyaloshinsky, J. Phys. Chem. Solids **4**, 241 (1958).
[11]T. Moriya, Phys. Rev. Lett. **4**, 228 (1960).
[12]J. Cho, N. H. Kim, S. Lee, J. S. Kim, R. Lavrijsen, A. Solignac, Y. Yin, D. S. Han, N. J. van Hoof, H. J. Swagten, B. Koopmans, and C. Y. You, Nat. Commun. **6**, 7635 (2015).
[13]A. A. Stashkevich, M. Belmeguenai, Y. Roussigné, S. M. Cherif, M. Kostylev, M. Gabor, D. Lacour, C. Tiusan, and M. Hehn, Phys. Rev. B **91**, 214409 (2015).
[14]A. Fert and P. M. Levy, Phys. Rev. Lett. **44**, 1538 (1980).
[15]S. Heinze, K. Bergmann, M. Menzel, J. Brede, A. Kubetzka, R. Wiesendanger, G. Bihlmayer, and S. Blügel, Nat. Phys. **7**, 713 (2011).
[16]H. Jia, B. Zimmermann, and S. Blügel, Phys. Rev. B **98**, 144427 (2018).
[17]H. Jia, B. Zimmermann, G. Michalicek, G. Bihlmayer, and S. Blügel, Phys. Rev. Mater. **4**, 024405 (2020).
[18]I. M. Miron, T. Moore, H. Szambolics, L. D. Buda-Prejbeanu, S. Auffret, B. Rodmacq, S. Pizzini, J. Vogel, M. Bonfim, A. Schuhl, and G. Gaudin, Nat. Mater. **10**, 419 (2011).
[19]T. A. Moore, I. M. Miron, G. Gaudin, G. Serret, S. Auffret, B. Rodmacq, A. Schuhl, S. Pizzini, J. Vogel, and M. Bonfim, Appl. Phys. Lett. **93**, 262504 (2008).
[20]Y. Chen, Q. Zhang, J. Jia, Y. Zheng, Y. Wang, X. Fan, and J. Cao, Appl. Phys. Lett. **112**, 232402 (2018).
[21]Y. Ou, C. F. Pai, S. Shi, D. C. Ralph, and R. A. Buhrman, Phys. Rev. B **94**, 140414(R) (2016).
[22]R. Ramaswamy, X. Qiu, T. Dutta, S. D. Pollard, and H. Yang, Appl. Phys. Lett. **108**, 202406 (2016).
[23]W. Skowroński, M. Cecot, J. Kanak, S. Ziętek, T. Stobiecki, L. Yao, S. V. Dijken, T. Nozaki, K. Yakushiji, and S. Yuasa, Appl. Phys. Lett. **109**, 062407 (2016).
[24]Y. Ishikuro, M. Kawaguchi, N. Kato, Y. C. Lau, and M. Hayashi, Phys. Rev. B **99**, 134421 (2019).
[25]H. T. Nembach, J. M. Shaw, M. Weiler, E. Jué, and T. J. Silva, Nat. Phys. **11**, 825 (2015).
[26]M. Belmeguenai, J. P. Adam, Y. Roussigné, S. Eimer, T. Devolder, J. V. Kim, S. M. Cherif, A. Stashkevich, and A. Thiaville, Phys. Rev. B **91**, 180405(R) (2015).
[27]N. Kato, M. Kawaguchi, Y. C. Lau, T. Kikuchi, Y. Nakatani, and M. Hayashi, Phys. Rev. Lett. **122**, 257205 (2019).
[28]T. Tanaka, H. Kontani, M. Naito, T. Naito, D. S. Hirashima, K. Yamada, and J. Inoue, Phys. Rev. B **77**, 165117 (2008).
[29]H. Kontani, T. Tanaka, D. S. Hirashima, K. Yamada, and J. Inoue, Phys. Rev. Lett. **102**, 016601 (2009).
[30]D. Go, D. Jo, C. Kim, and H. W. Lee, Phys. Rev. Lett. **121**, 086602 (2018).
[31]D. Jo, D. Go, and H. W. Lee, Phys. Rev. B **98**, 214405 (2018).
[32]T. Y. Chen, H. I. Chan, W. B. Liao, and C. F. Pai, Phys. Rev. Appl. **10**, 044038 (2018).
[33]T. C. Chuang, C. F. Pai, and S. Y. Huang, Phys. Rev. Appl. **11**, 061005 (2019).
[34]Z. C. Zheng, Q. X. Guo, D. Jo, D. Go, L. H. Wang, H. C. Chen, W. Yin, X. M. Wang, G. H. Yu, W. He, H. W. Lee, J. Teng, and T. Zhu, Phys. Rev. Res. **2**, 013127 (2020).
[35]Z. Wen, J. Kim, H. Sukegawa, M. Hayashi, and S. Mitani, AIP Adv. **6**, 056307 (2016).
[36]H. Wu, S. A. Razavi, Q. Shao, X. Li, K. L. Wong, Y. Liu, G. Yin, and K. L. Wang, Phys. Rev. B **99**, 184403 (2019).
[37]T. Shang, Q. F. Zhan, L. Ma, H. L. Yang, Z. H. Zuo, Y. L. Xie, H. H. Li, L. P. Liu, B. M. Wang, Y. H. Wu, S. Zhang, and R. W. Li, Sci. Rep. **5**, 17734 (2015).
[38]J. Finley, C. H. Lee, P. Y. Huang, and L. Liu, Adv. Mater. **31**, 1805361 (2019).
[39]J. Kim, J. Sinha, M. Hayashi, M. Yamanouchi, S. Fukami, T. Suzuki, S. Mitani, and H. Ohno, Nat. Mater. **12**, 240 (2013).
[40]M. Hayashi, J. Kim, M. Yamanouchi, and H. Ohno, Phys. Rev. B **89**, 144425 (2014).
[41]Q. Hao and G. Xiao, Phys. Rev. B **91**, 224413 (2015).
[42]A. F. Mayadas and M. Shatzkes, Phys. Rev. B **1**, 1382 (1970).
[43]M. H. Nguyen, D. C. Ralph, and R. A. Buhrman, Phys. Rev. Lett. **116**, 126601 (2016).
[44]W. Zhang, W. Han, X. Jiang, S. H. Yang, and S. S. P. Parkin, Nat. Phys. **11**, 496 (2015).
[45]K. Di, V. L. Zhang, H. S. Lim, S. C. Ng, M. H. Kuok, J. Yu, J. Yoon, X. Qiu, and H. Yang, Phys. Rev. Lett. **114**, 047201 (2015).
[46]J. Yu, X. Qiu, Y. Wu, J. Yoon, P. Deorani, J. M. Besbas, A. Manchon, and H. Yang, Sci. Rep. **6**, 32629 (2016).
[47]X. Ma, G. Yu, X. Li, T. Wang, D. Wu, K. S. Olsson, Z. Chu, K. An, J. Q. Xiao, K. L. Wang, and X. Li, Phys. Rev. B **94**, 180408(R) (2016).
[48]X. Ma, G. Yu, C. Tang, X. Li, C. He, J. Shi, K. L. Wang, and X. Li, Phys. Rev. Lett. **120**, 157204 (2018).